Lasers in Manufacturing Conference 2025

Surrogate Model-Based Optimization: Utilizing Neural Networks to Benchmark Process Parameter Development Strategies for Laser Polishing of Metals

Ley, Vincent Benedikt [a,b]; Linden, Sven [a,b]; Kuepper, Moritz [b]; Willenborg, Edgar[b]

[a] *Chair for Technology of Optical Systems TOS, RWTH Aachen University, Steinbachstraße 15, 52064 Aachen, Germany*
[b]*Fraunhofer Institute for Laser Technology, Steinbachstraße 15, 52064 Aachen, Germany*

Abstract

Laser polishing of metals is a multi-step process requiring detailed and individual parameter optimization for each processing step. The experimental approach to parameter optimization for new materials and initial surface roughness is not optimized itself. Therefore, high numbers of experiments are necessary. Furthermore, established approaches neglect that laser polishing is a multi-step process, resulting in redundant experimentation and suboptimal roughness. In this work, a new approach for optimizing and benchmarking the parameter optimization process is developed. This approach is based on a surrogate model using a dataset of 2,560 conducted experiments on laser polishing of AISI H11. By using the surrogate model, efficient and low-cost optimization and comparison of parameter optimization strategies are enabled. In the benchmark, a wide range of conditions, such as sample limitation and target roughness, were tested. As a result, the domain-based approach could find parameters meeting the criteria in less than 50 experiments even for a suboptimal choice of initial process parameterization fed to the algorithm.

Keywords: Laser polishing, metals; process parameter development; neural networks; low-cost optimization

Nomenclature: Laser polishing of metals: LPM, Process parameter development: PPD, Design of experiments: DOE

1. Introduction

As of now, mechanical polishing represents the state of the art in the final processing of components for the aerospace and automotive industries, medical technology, and tool and mold making, among others. A primary objective of polishing is to reduce the initial roughness. Complex 3D geometries are often polished manually in an expensive and lengthy process. [Zeng et al., 2023; Gisario et al., 2022]

Laser polishing of metals (LPM) is an automated alternative to mechanical polishing methods. The remelting of a thin surface layer during LPM allows for the mitigation of the workpiece's initial roughness, where the redistribution of the material in the molten state and subsequent smoothing of the surface are attributed to interfacial tension. In this work the LPM process known as macro-polishing is focused, which utilizes continuous laser radiation. Macro-polishing typically uses laser beam diameters from 100 µm up to 600 µm and in return reduces surface structures of higher structural wavelength range λ_s. This approach stands in contrast to the process of micro-polishing, which utilizes pulsed laser radiation using smaller laser beam diameters (25 - 100 µm). Micro-polishing mitigates surface structures with structural wavelengths λ_s below 100 µm. Consequently, micro-polishing has been demonstrated to enhance the gloss level of the processed surface. According to the state of art, LPM is a multi-stage process, thus two macro-polishing steps with refining process parameters are necessary to achieve lowest surface roughness. An optional micro-polishing step may also be incorporated. [Willenborg, 2005; Temmler et al., 2020; Kiedrowski, 2009]

For macro-polishing, the laser beam is directed in a meandering pattern across the surface using a laser scanner. In the context of macro-polishing, the reduction in initial roughness is found to be significantly influenced by the following process

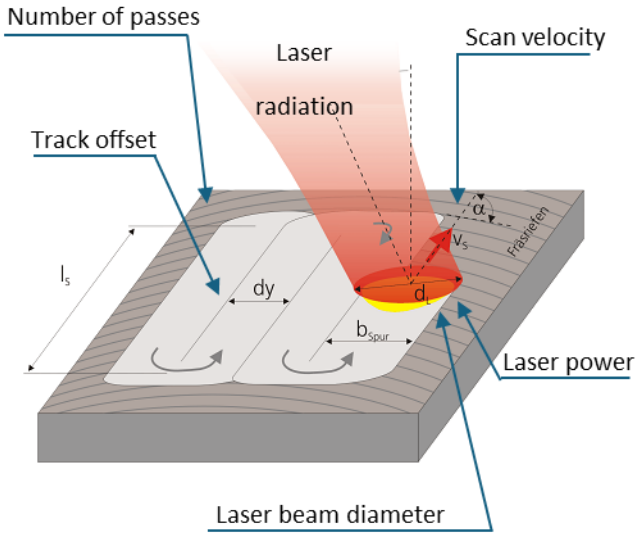

Figure 1: LPM using continuous wave laser radiation and process parameter dimensions considered in this work. [Willenborg, 2005]

parameter dimensions, which are the focal point of this study: laser beam diameter d_L, laser power P_L, scanning speed v_s, track offset dy, number of passes n, and processing direction α. A combination of these process parameter dimensions is recorded as a process parameter set. It should be noted that the variation of other process parameter dimensions, such as the selection of inert gas utilized to prevent oxidation of the surface (e.g. Ar, He, N), is not being taken into consideration in this work. LPM is shown schematically in Figure 1 alongside investigated parameter dimensions. [Temmler et al., 2020; Kumstel, 2021]

While LPM facilitates the automated processing of complex 3D geometries, its application is constrained by achievable reduction in initial roughness, potentially induced waviness and extended processing times. Due to the non-linear thermo-physical interaction between process, laser and material, extensive process parameter development (PPD) is conducted to find suitable candidates of process parameters among local optima (referred to as LPM-PPD hereafter). The LPM process is dependent on the material and initial surface roughness, the parameterization of laser and scanner and the workpiece's geometry. Depending on prior experimental findings and knowledge on LPM of given material and subsequent conditions, referred to as domain knowledge hereafter, between 100 to 300 experiments are found to determine suitable process parameter sets. This results in a significant investment of time and costs. [Willenborg, 2005; Temmler et al., 2020]

To help reduce the number of redundantly tested process parameter sets, LPM-PPD must increase efficiency. Efficiency is measured by the number of process parameter sets evaluated or the duration of LPM-PPD measured as time. Effectiveness describes the attribute of LPM-PPD being able to find a process parameter set suitable for the objective at hand. Aiming at an increase in efficiency and effectiveness, different LPM-PPD strategies are developed and employed. These strategies are built upon one or a combination of these three components, depending on the financial resources and time available: domain knowledge, design of experiments (DOE), and physical or data-based modeling.

The central objective is to demonstrate that domain knowledge improves reducing the number of experimental investigations whilst being able to search within greater number of process parameter dimensions than in purely statistical analyses. An implementation of an LPM-PPD strategy with DOE and use of domain knowledge is developed. The approach is compared to purely statistical DOE methods in a benchmark.

However, in the context of experimental investigations, a benchmark of process parameter development strategies entails a substantial investment of time and financial resources, particularly given the iterative nature of the comparison of the examined strategies and number of process parameter sets. To address this, costly real-world experiments will be replaced by a surrogate model serving as an approximate substitute. The results predicted by the surrogate model can then be used to benchmark LPM-PPD strategies, enabling efficient and low-cost, albeit approximate, comparison and optimization. The model error will be analysed to assess the reliability of the strategy comparison. Within a benchmark effectiveness and efficiency of the strategies will be evaluated. This allows for the selection of an optimal LPM-PPD strategy among the benchmarked candidates. An outcome of this work is a standardized, domain-knowledge-driven strategy for LPM-PPD that can be applied to future process parameter development efforts.

1.1. Surrogate modelling for design space optimization

Surrogate modeling, or metamodeling, refers to the construction of data-driven approximations that emulate the behavior of complex simulations or physical systems, often built using empirical function approximation techniques [Wang, 2007]. These models reduce computational cost while maintaining sufficient accuracy, making them valuable for scenarios involving expensive or time-consuming evaluations [Simpson, 2001; Forrester et al., 2008]. Surrogates support parallel data generation, filter out numerical noise, and offer global approximations useful for sensitivity analysis and design exploration. However, they involve trade-offs in accuracy, especially if the input space is poorly covered, which can lead to misleading conclusions about system behavior.

Polynomial regression offers a simple and interpretable approximation, suitable for smooth problems but often limited in capturing complex nonlinearities [Bhosekar and Ierapetritou, 2018]. Regression trees partition the input space to model local behavior effectively and handle variable interactions, though they may produce discontinuous outputs and risk overfitting [Mišić, 2020]. Neural networks provide high flexibility and can approximate highly nonlinear functions, including multi-output cases, but require tuning to avoid overfitting and can be challenging to embed within optimization frameworks [Fischetti and Jo, 2018; Grimstad and Andersson, 2019]. Gaussian processes are probabilistic models that deliver both predictions and uncertainty estimates, making them ideal for small datasets and robust optimization, though their scalability is limited in high-dimensional or data-rich settings [Bertsimas et al., 2010; Wilson et al., 2020]. Each surrogate type involves trade-offs between model complexity, interpretability, scalability, and integration into optimization workflows.

Surrogate-based optimization strategies are traditionally framed within either the surrogate-led or mathematical programming-led perspectives [Bhosekar and Ierapetritou, 2018; McBride and Sundmacher, 2019; Misener and Biegler, 2023]. The former selects a surrogate model based on system properties, while the latter chooses a model to meet optimization constraints such as linearity or convexity. However, in this work, the design space of LPM-PPD is precisely defined and limited. Therefore, deviation from both traditional approaches is possible. The primary purpose of the surrogate model is to emulate the real process in a full LPM-PPD loop across multiple LPM-PPD strategies, enabling systematic benchmarking of strategy performance. The objective is to identify the most effective LPM-PPD for the specific setting at hand. Rather than high accuracy of the surrogate's optimum solely within the true process optimum, high accuracy across the entire design space is required. This is critical due to multiple iterations of LPM-PPD evaluating different process parameter sets. If the surrogate model error is large in regions outside the optimum, the surrogate model may mislead the LPM-PPD strategy and compromise the evaluation. Therefore, the selection of a surrogate model with low global predictive error is the focus of this work, ensuring that iterative evaluations remain trustworthy throughout LPM-PPD.

1.2. Process parameter development for laser polishing of metals

Domain knowledge in LPM-PPD can be used for limiting the examined process parameter space, choosing a starting point for PPD and interpreting results during PPD in the search of a global optimum. As a key novelty of this work, domain knowledge can further be leveraged to examine process parameter dimensions independently by defining a sequential variation approach. This sequence ensures that the determined properties of remelting of the thin surface layer are not influenced in subsequent variation of process parameter dimensions. [Willenborg, 2005; Kiedrowski, 2009; Kumstel 2021]

In contrast to the sequential variation approach, state-of-the-art LPM-PPD strategies typically employ DOE techniques that vary multiple process parameter dimensions simultaneously. To reduce the scope of experimental investigations, process parameter sets are selected on a statistical basis. The individual influence of the process parameter dimensions is only given a subordinate role. However, a uniform DoE is not consistently applied across all cases. A variety of methodologies are employed, with the most prevalent being a full factorial combination and a 2k-factorial design. [Ukar et al., 2008; Kumar et al., 2025; Solheid et al., 2020; Rosa et al., 2014; Meylan et al., 2022]

Physical modeling reduces the scope of LPM-PPD through approximative simulations. Often, this involves approximating a heat conduction equation to simulate the dynamics of the melt pool. However, this approach is often limited to a subset of parameter dimensions as restricted by physics. For example, melt pool temperature is simulated through variation of P_L and v_s. Also, these simulations require considerable time and computing power, and their accuracy depends on how well the physics are modelled and the conditioning of simulation matches the real-world conditions (material, initial roughness, etc.). [Ukar et al., 2012; Solheid et al., 2022; Meylan et al., 2022; Pham et al., 2024]

The utilization of DOE has emerged as the predominant LPM-PPD strategy. The integration of domain knowledge into LPM-PPD is frequently disregarded and its sole purpose often is to identify a starting process parameter set for DOE. In most cases, the scope of experimental investigations is severely limited by varying only a few process parameter dimensions, selecting a small number of process parameter sets (usually fewer than 50, often 10 to 20) or using only few iterations i during LPM-PPD with $i = 1$ being the most common. [Gisario et al., 2022; Temmler et al., 2020]

2. Method

2.1. Domain-knowledge driven data set for LPM of AISI H11

To create the surrogate model for LPM, a data set is compiled based on extensive real-world experiments on LPM of AISI H11 chosen in accordance with the detailed investigations of E. Willenborg and T. Kiedrowski. The process parameter sets determined for the data set contain both optimal and suboptimal process parameters for LPM of AISI H11 to examine the whole process parameter space.

The experimental investigation is conducted on 20 discs of AISI H11 (diameter of 162 mm, thickness of 20 mm). Up to 147 process parameter sets per disc with field size of 10 mm x 10 mm are processed in rings of increasing radii. LPM is conducted using argon as inert gas. Residual oxygen content was measured and is held at 1,000 ppm by use of a control system. Prior to LPM the discs are processed by turning with a groove distance of 200 µm. Therefore, the dominant influence on the initial roughness refers to the primary roughness wavelength λ_s = 200 µm. A low variance of initial roughness throughout the 20 discs is ensured by cutting all discs from a single round blank and consistent turning parameters. A photography of an AISI H11 disc with several samples is shown in Figure 2 (a).

The investigated parameter space is divided into discrete levels which are combined full-factorially. Table 1 gives an overview of the calculation for the process parameter space, where rules are to be applied sequentially from the topmost parameter in the table to the bottommost and combined full-factorially. This results in a total of 2,560 unique process parameter sets. The levels of subsequent process parameter dimensions are derived from d_L = 250 µm. If the laser beam diameter differs, levels for subsequent dimensions must be adapted based on the formulas shown in the comment column. The choice of process parameter range and levels is explained in the following list:

Table 1. Process parameters and rules to calculate parameter space for full-factorial combination with d_L= 250 µm being the default laser beam diameter on which the ranges of subsequent process parameters have been applied to.

Process parameter	**Symbol**	**Unit**	**Range**	**Levels**	**Comment**
Laser beam diameter	d_L	µm	[100, 150, 250, 400, 600]	5	Approximately 150-160% between levels
Laser power	P_L	Watt	[50, 60 74, 90 ,110, 134, 164, 200] × f_{d_L}	8	$f_{d_L} \coloneqq \frac{d_L}{250}$, $P_{L_{base}} \coloneqq \frac{d_L}{2.5}$, $P_L \leq 500$ Watt
Scan velocity	v_s	mm/s	[25, 35, 49, 70, 99, 140, 198, 279] × f_{P_L}	8	$f_{P_L} \coloneqq \frac{P_L}{P_{L_{base}}}$, $v_s \geq 25$ mm/s
Track offset	dy	µm	[0.1, 0.2, 0.4] × d_L	3	Empirical value often at 0.25
Number of passes	n	-	[1,2,4]	3	

- Starting with the laser beam diameter, five levels are selected for d_L. Initially, d_L = [250, 400] µm are examined as these values are close to the suggested domain-knowledge driven value $d_L \geq 200$ µm. Furthermore, an increase to d_L = 600 µm is examined at which a substantial increase in waviness is anticipated resulting in potentially more suboptimal values. Additionally, the data set entails values of d_L = [100, 150] µm at which incomplete remelting of the dominant surface structure is expected, attributed to insufficient width of the melt pool.
- P_L is adjusted in eight levels corresponding to d_L. According to the process parameters established by T. Kiedrowski, P_L = 100 W is utilized as the baseline for d_L = 250 µm. Starting from this baseline, P_L is adapted linearly to changes in d_L. Within the parameter space of the individual d_L, P_L is systematically varied in increments of 1.22. This allows for detailed examination of the resulting parameter spaces. Low values of P_L are examined to detect insufficient remelting of the thin surface layer, while high values of P_L result in overmelt and further carbonization of the surface.
- v_s is varied in eight levels. The selection of levels is based on P_L. The lower limit is set v_s = 25 mm/s to limit the increase in processing time.
- dy subject to identical variation across all parameter spaces in range of [0.1, 0.2, 0.4], independent of the preceding process parameters. The levels of dy = [0.1, 0.2] × d_L are adopted from domain knowledge to achieve a substantial reduction in initial roughness. Furthermore, the investigation encompasses dy = 0.4 × d_L, aiming to decrease processing time whilst ensuring sufficient roughness reduction.
- Lastly, the variation of n = [1, 2, 4] is examined. According to domain knowledge, increasing n results in a further reduction of the initial roughness. In contrast, n = 1 is examined to include a minimal processing time.

During experiments with d_L = [250, 400, 600] µm a redPower QUBE 500 fiber laser by SPI Lasers UK Ltd (max. laser power of $P_{L,max}$ = 500 W, laser wavelength of λ = 1064 nm) is used. LPM with these smaller d_L = [100, 150] µm is processed utilizing

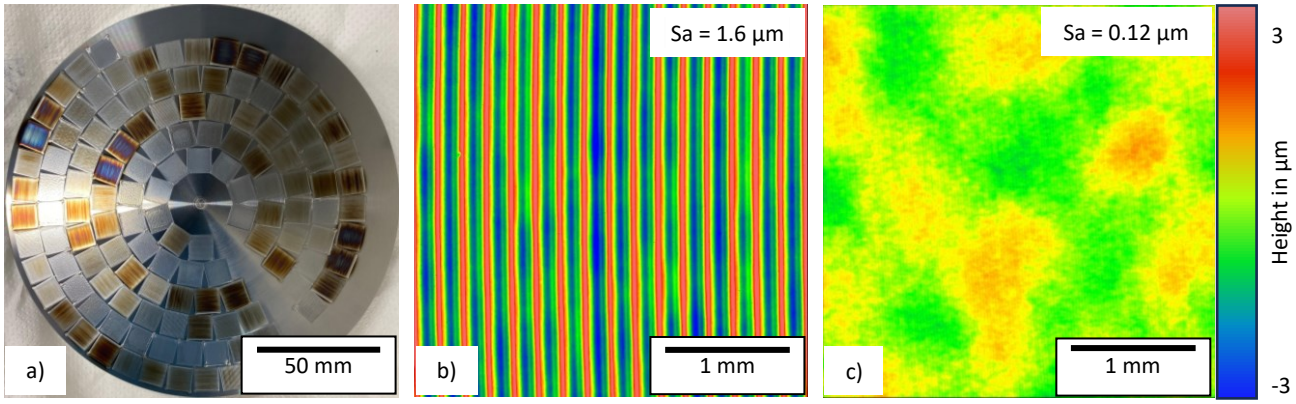

Figure 2: (a) Image showing multiple samples of LP on an AISI H11 disc. (b) Surface profile before and (c) after processing by LPM recorded with WLI.

a YLPN 200-R fiber laser by IPG Photonics Corporation ($P_{L,max}$ = 200 W, λ = 1080 nm). The individual adjustment of d_L is achieved through a proprietary optomechanical setup, which is described in detail by A. Temmler in [Temmler et al., 2020] In this configuration, a zoom telescope is employed along the beam path, preceding the deflection of laser radiation through a HurryScan 30 by SCANLAB GmbH.

The measurement results stored in the data set are obtained by measuring the surface profile of the samples using a white light interferometer (WLI) NX2 from AMETEK Germany GmbH, BU Zygo. The measurements are obtained at magnifications of 1.4x, 2.5x, 10x, and 50x. An example of surface profiles recorded using WLI at 2.5x magnification is shown in Figure 2(b) and (c) comparing initial roughness to roughness after LPM with respective Sa value.

To assess the reduction in initial roughness, the surface roughness value *Sa* is calculated as the mean arithmetic height from the measurement of the surface profile in accordance with DIN EN ISO 25178 [DIN EN ISO 25718, 2016]:

$$Sa = \frac{1}{A}\iint_A |z(x,y)|dxdy\,, [Sa] = \mu m \qquad (1)$$

Additionally, the data set provides the short-, medium-, and long-wave proportions of the surface profile via filtered Sa values. These are generated by applying a low-pass filter or a band-stop filter to the WLI measurement data. In the process, the cut-off wavelength λ_c of the filter is selected in accordance with DIN EN ISO 21920-3 [DIN EN ISO 21930-3, 2022]. The designations of the filtered Sa values and corresponding λ_c are enumerated in Table 2. In this study, the surface profile is examined using the Sa-SL value to mitigate the impact of shape deviations on the surface of the samples. Sa-SL encompasses both the roughness and the waviness of the surface. In instances where the surface profile of a specimen is evaluated based on its waviness, the Sa-L value is employed as a metric. Finally, the short-wave roughness is specified in relation to the reduction in the initial roughness as Sa-S. The mean values for initial roughness and initial waviness of the samples before LPM are Sa-S = 1.57 µm and Sa-L = 0.1 µm.

Table 2. Filtered Sa-values with associated cut-off wavelengths to assess different proportions of the surface profile.

Designation	λ_c in µm	Filter type	Considered proportion of the surface profile	Mean values in data set before LPM in µm
Sa-S (Short)	[2.5, 800]	band-pass	roughness	1.57
Sa-L (Long)	[800, 2500]	band-pass	waviness	0.1
Sa-SL	2500	low-pass	roughness and waviness	1.6

2.2. Machine learning methodology for surrogate model

To construct a robust and generalizable surrogate model using a multi-layer perceptron (MLP), a comprehensive machine learning workflow was implemented. This workflow incorporates best practices in data preprocessing, model architecture design, training, validation, and performance evaluation, with the goal of minimizing overfitting and maximizing predictive accuracy. In addition to the MLP, alternative modeling approaches, including polynomial regression, kernel-based methods, and Gaussian processes, were also explored. However, these alternatives demonstrated inferior performance. The workflow begins with data preprocessing, where input and output features are selected and scaled using a custom standard scaler.

The data set described above is then split into three parts: 70% for training (1792 data points), 15% for validation, and 15% for testing (384 data points each). The workflow is implemented in Python 3.13 using PyTorch and numpy.

A hyperparameter optimization is conducted via grid search. A variety of architectural and training parameters are explored, including hidden layer count, hidden units, learning rate, dropout rate, and weight decay. Each configuration is evaluated across consistent train/validation splits, and the best set of parameters is identified based on validation root-mean squared error (RMSE). To prevent overfitting during training, early stopping and learning rate scheduling are employed. Dropout layers are inserted between dense layers as a form of regularization, reducing neuron co-dependence. Weight decay (L2 regularization) further discourages overfitting by penalizing large weights.

A grid search was conducted across 576 hyperparameter configurations. The final model, chosen based on lowest validation RMSE, demonstrated strong generalization on the test set with MSE = 0.027 µm², RMSE = 0.164, and MAE = 0.087. The chosen hyperparameters are shown in Table 3. The dropout rate did not improve the model and is removed from the table.

Table 3. Hyperparameters chosen for multi-layer perceptron.

Hyperparameter	**Hidden layers**	**Hidden units**	**Activation Function**	**Learning rate**	**Max epochs**	**Weight decay**
Value	5	100	ReLu	0.001	500	0.0001

In the following analysis of the model performance, the relative model error $\epsilon_{rel}$is used as it quantifies the error independently of the true absolute values. This allows for a consistent and comparable assessment of model performance across the entire range of predicted Sa values. In this regard, $(x_\mathrm{i}, \mathrm{y_i})$ is the process parameter set and response of the real-world experiment whereas $\mathrm{y_i^*}$ is the model prediction for x_i:

$$\epsilon_{rel} = \frac{abs(y_i - y_i^*)}{y_i} \cdot 100\,, [\epsilon_{rel}] = \% \qquad (2)$$

Table 4 summarizes key statistical metrics of the relative model error across different laser beam diameters, including mean, standard deviation, median, and extreme values. In several parameter regimes, the median error is notably lower than the mean, for example, at d_L = 150 µm, the mean error is 21.02%, whereas the median is only 10.98%. This discrepancy indicates a positively skewed error distribution, where a small number of large deviations inflate the mean. Similar trends are observed for d_L = 250 µm and d_L = 600 µm, suggesting that most predictions are relatively accurate, with a few outliers contributing disproportionately to the overall error. d_L = 400 µm, while showing the highest standard deviation (42.84%), also exhibits a low median error (6.34%), reinforcing this observation. These findings suggest that the surrogate model delivers robust and generally accurate predictions across most of the parameter space, with large errors being rare and identifiable.

Table 4. Statistics on relative model error in percent grouped by the laser beam diameter and overall mean value for each statistic.

Laser beam diameter in µm	**Mean relative error in %**	**Standard deviation relative error in %**	**Median of relative error in %**	**Minimal relative error in %**	**Maximal relative error in %**
100	8.97	11.79	7.52	0.01	45.45
150	21.02	7.65	10.98	0.41	266.94
250	16.65	17.57	11.87	0.43	94.96
400	10.92	42.84	6.34	0.19	54.37
600	14.36	18.89	9.89	0.05	124.92
Mean (All)	**14.39**	**19.75**	**9.32**	**0.22**	**117.38**

Figure 3 and Figure 4 visualize the multi-layer perceptron's surface roughness predictions Sa-S and corresponding relative model errors ϵ_{rel} across the process parameter space defined by laser power P_L and scan speed v_s. This process parameter space is shown separately for two selected laser beam diameters (d_L = 250 µm and d_L = 600 µm) with constant values of dy = 0.2 × d_L and n = 2. Warmer colors indicate higher predicted surface roughness, while cooler colors correspond to smoother surfaces and for model error analogous. The roughness maps (left panels) show a consistent trend where increased laser power and decreased scan speed result in smoother surfaces, with a clear threshold for laser power P_L to access regions of low roughness. This threshold shifts upward with increasing d_L, consistent with domain expectations.

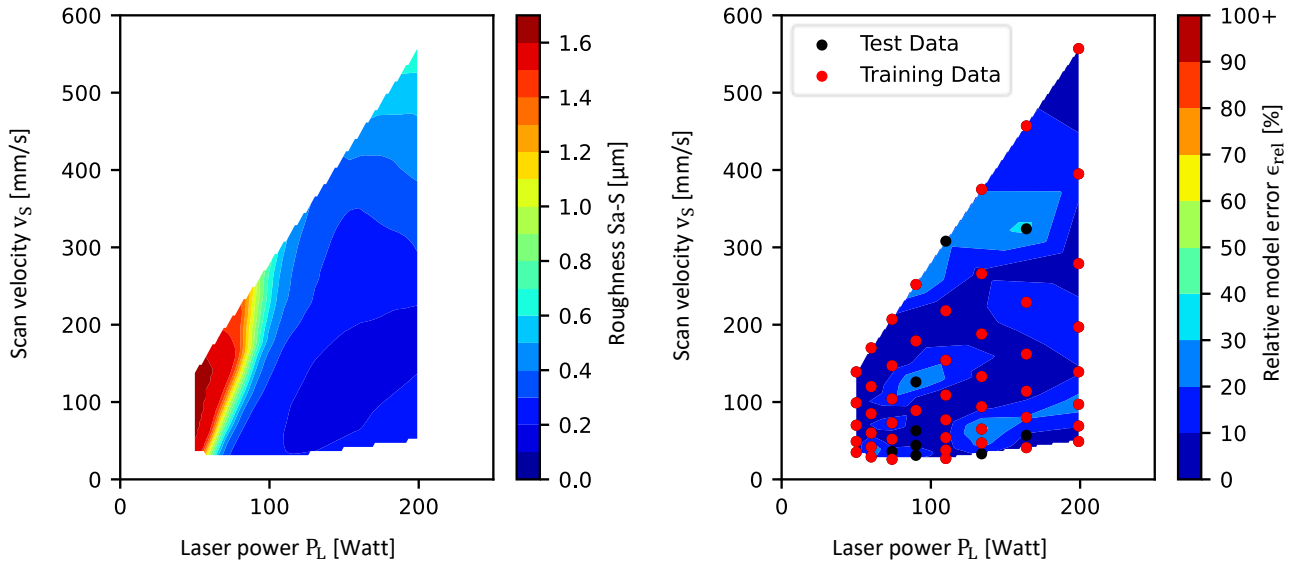

Figure 3: (Left) Heat map of Sa values for P_L and v_s predicted by surrogate model for d_L = 250 µm, dy = 50 µm, n = 2. (Right) Heat map of relative model error ϵ_{rel} for d_L = 250 µm, dy = 50 µm, n = 2 computed for test and training data. Relative model error is capped between [0, 100].

The error maps (right panels), capped between values of 0% and 100%, show that most predictions lie within a relative error of 0–30%, with higher errors occurring in under-sampled or highly nonlinear regions. Training and test data overlay demonstrates that the model error is decreased in highly sampled regions, while sparse regions contribute disproportionately to higher errors.

These visualizations confirm the surrogate model's reliable interpolation performance and identify areas for potential refinement through targeted data augmentation. For example, at d_L = 600µm, two extreme points of high model error are observed in the region of low to medium laser power and low to medium scan speed, corresponding to an area of high non-linearity in the model's predicted roughness response.

Given the inherent approximations involved in surrogate modeling, such skewed but bounded error behavior is acceptable, particularly when the model is used for tasks such as design exploration, sensitivity analysis, or optimization. Overall, the results (Median relative model error = 9.32 %) support the model's usability as a computationally efficient surrogate, capable of providing reliable estimates while enabling uncertainty-aware decision-making. It should be noted that the final determined process parameter set should be verified by real experiments.

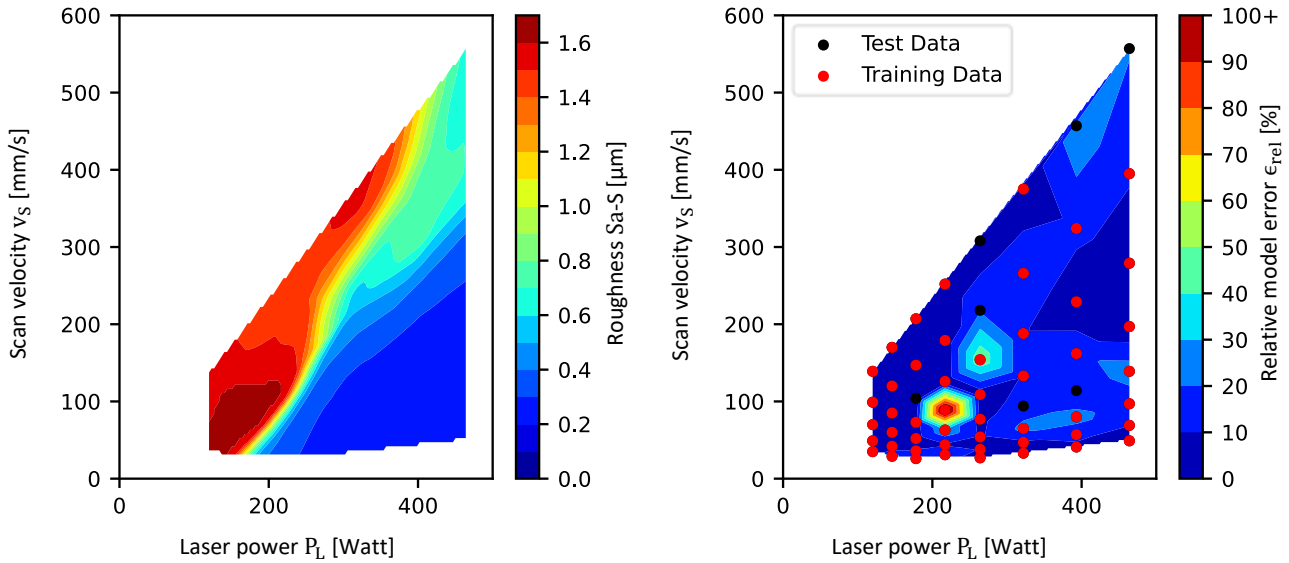

Figure 4: (Left) Heat map of Sa values for P_L and v_s predicted by surrogate model for d_L = 600 µm, dy = 120 µm, n = 2. (Right) Heat map of relative model error ϵ_{rel} for d_L = 600 µm, dy = 120 µm, n = 2 computed for test and training data. Relative model error is capped between [0, 100].

2.3. Domain knowledge on the variation of process parameters in LPM

In the work of E. Willenborg, extensive LPM-PPD based on domain knowledge and individual variation of process parameter dimensions is conducted. The experimental investigations are carried out on samples of AISI H11 that are prepared by turning. A wide range of process parameter sets is investigated, without constraining a narrow parameter space beforehand. The minimal surface roughness that can be achieved by LPM of AISI H11 is influenced by the quality of the workpiece. Adding to the methodology of E. Willenborg, T. Kiedrowski investigates the formation of surface structures depending on process parameters during LPM and their subsequent elimination. A surface roughness of Ra = 0.05–0.1 µm is achieved. The process parameter set determined in this study is listed in Table 1. [Willenborg, 2005; Kiedrowski, 2009]

Table 5. Process parameter set determined by T. Kiedrowski for LPM of AISI H11 for reduction in initial roughness in relation to turning grooves with distance of 200 µm. [Kiedrowski, 2009]

d_L in µm	P_L in W	v_s in mm/s	dy in µm	n
240	100	110	60	10

Based on E. Willenborg and T. Kiedrowski, the following rules for determining the process parameter dimensions separately are recorded as domain knowledge:

- The **processing direction** $\boldsymbol{\alpha}$ is set perpendicular to the dominant surface structure from previous processing steps (e.g. turning grooves). To ensure the homogeneous redistribution of the material and the elimination of directional surface structures, α is rotated by 90° between passes.
- Increases in the **beam diameter** $\boldsymbol{d_L}$ result in wider melt pools. Therefore, d_L is chosen depending on λ_s of the primary surface structure:

$$d_L \geq \lambda_s \tag{3}$$

  However, an increase in d_L should be limited to prevent an increase in waviness.
- Increasing the **laser power** $\boldsymbol{P_L}$ results in an increase in melt volume, thereby enhancing the reduction in the initial roughness. It is essential that P_L be sufficiently high so that a stable melt pool with minimal fluctuations in the melt volume can be achieved. The upper limit of P_L is constrained to prevent decarburization of the thin surface layer and vaporization of the material. P_L is adjusted proportionally to a change in d_L to keep the irradiance (approximatively) constant.
- Similarly, a reduction in the **scanning speed** $\boldsymbol{v_s}$ corresponds to higher energy density and thus an increase in melt volume. The reduction in v_s is limited by the evaporation temperature. The economic viability of LPM is another lower limit.
- A further reduction in the initial roughness is attributed to the process of repeated local remelting. This is realized through a decrease of the **track offset** $\boldsymbol{dy}$, which is limited by the increase in processing time and economic viability of LPM. According to the works of E. Willenborg and T. Kiedrowski, dy is determined as 10%, 20% or 25% of d_L. To ensure that individual tracks overlap, $dy < d_L$ is set. dy is adjusted proportionally when d_L is changed, if other process parameters remain constant.
- Additionally, repeated local remelting is achieved by an increase in **number of passes** $\boldsymbol{n}$. E. Willenborg states that the lower limit should be set at $n = 2$. The upper limit of n is determined by balancing economic viability of LPM with roughness reduction.

Using the sequence listed above ($d_L \rightarrow \{P_L, v_S\} \rightarrow \{dy, n\}$), process parameter dimensions can be investigated sequentially with only a subset being varied. In this regard, the investigation of a process parameter dimension does not significantly influence process parameter dimensions prior in the sequence. The properties of the remelting of the thin surface layer which are adjusted by the process parameter dimensions are listed below as described by [Willenborg, 2005; Kiedrowski, 2009]:

- To ensure the remelting of the dominant surface structures, it is necessary to establish the process parameter dimensions that determine melt pool width and melt volume first. Therefore, d_L is set as the first process parameter dimension and chosen in accordance with the structural wavelength λ_s of the initial surface.
- The melt volume is adjusted through P_L and v_s. First, the process parameter dimension of P_L and v_s for the determined d_L is searched with a “rough” variation and large distances between varied process parameter sets. Then, a “fine” variation with smaller distances is performed around the local optimum determined for the reduction in initial roughness.
- dy is calculated based on d_L. The value is chosen in descending order from [0.1, 0.2, 0.4] × d_L

- n is varied by doubling its current value.
- Lastly, a decrease of d_L is investigated to attain a similar reduction in roughness with even smaller d_L, avoiding an increase in waviness.

2.4. LPM-PPD based on domain knowledge

At the beginning of the LPM-PPD process, a starting parameter set is selected based on domain knowledge and the material properties being considered. Process parameter dimensions are then systematically and sequentially explored. During the variation of selected process parameter dimensions all other process parameter dimensions are kept constant. The attainment of a reduction in initial roughness is evaluated in relation to both excessive energy input and inadequate processing times. LPM-PPD based on domain knowledge follows the following rule set:

- In instances where the maximum number of allowable process parameter sets (e.g. restricted number of samples) has not yet been reached, a batch of process parameter sets is generated by full factorial combination of process parameter dimensions.
- If evaluated process parameter sets from prior variations are available, process parameter sets from the new batch are filtered. Filtering of new values in process parameter dimensions q_{new} is conducted based on examined values $q_{examined}$ and respective individual threshold t by:

$$|q_{new} - q_{examined}| \geq t \cdot q_{examined} \qquad (1)$$

- Subsequently, the batch of process parameter sets is investigated. The current best process parameter set of the batch is then identified – typically the one that achieves the lowest surface roughness. If this variation phase is effective, the LPM-PPD moves on to the next process parameter dimension. Otherwise, the current best process parameter set is adjusted and reused to refine the current process parameter dimension further.
- If the exploration of the current process parameter dimension reaches the predefined maximum number of allowable process parameter sets, further variations are limited by excluding less promising options. Specifically, process parameter sets with the greatest deviation from the current best process parameter set are removed. If the number of process parameter sets is still too high, further exploration of that process parameter dimension is stopped.

Depending on which process parameter dimension is investigated, different aspects of the surface profile are emphasized during selection of the current best process parameter set:

- In the “rough” variation of P_L and v_s the influence of LPM on surface roughness and waviness is considered.
- During the subsequent “fine” variation of P_L and v_s, among all process parameter sets that meet the target roughness, the one with the lowest waviness is chosen as the current best. This helps counteract the tendency of LPM to introduce new surface structures that increase waviness.
- In subsequent variations of dy and n as well as the decrease of d_L only the roughness is considered.

The underlying iterative and sequential process used in the LPM-PDD strategy based on domain knowledge is shown schematically using a flowchart in Figure 5.
It shall be noted that the complete strategy can be recreated applying the listed rule set into the flowchart with d_L as the first process parameter to be varied, then $\{P_L, v_s\}$, then dy and lastly n.

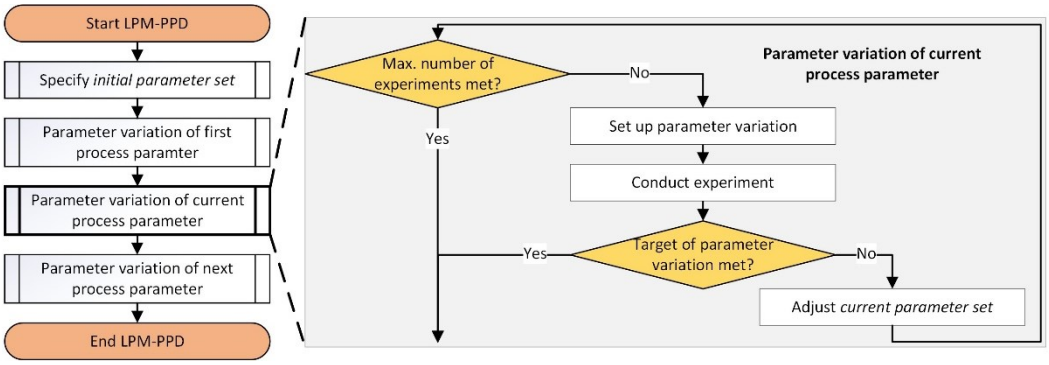

Figure 5: Flowchart giving an overview of the iterative and sequential LMP-PPD strategy based on domain knowledge.

3. Benchmarking process parameter development strategies using a surrogate model

For the evaluation and comparison of LPM-PPD strategies, a benchmark framework is developed. Figure 6 illustrates the structure, which enables systematic benchmarking. The benchmark framework integrates digitized LPM-PPD strategies, which propose process parameters, with a surrogate model that forecasts corresponding process results. These results are assessed against predefined performance targets such as surface roughness, processing time, personnel time, and material cost. The benchmark framework allows the incorporation of boundary conditions, including limits on process parameter ranges, processing time, or the number of allowable real experiments. By simulating multiple LPM-PPD runs for each strategy, the benchmark framework supports a comparative analysis of effectiveness and efficiency under varying constraints. In this context, the surrogate model replaces the need for costly or time-intensive real-world experiments, enabling robust strategy evaluation and ultimately facilitating the standardization and selection of suitable LPM-PPD strategies. Moreover, it allows for strategy hyperparameter tuning such as the number of process parameter dimensions and levels in case of a DOE based strategy. Additionally, the number of run experiments and the cumulative cycle time of LPM-PPD t_C are returned, where t_C remarks the fictional machine and metrology time for the complete list of process parameter sets.

t_C is composed of the processing time t_P and the auxiliary time t_A for each batch of process parameter sets. t_P is calculated based on the process parameter dimensions v_s, dy and n for a sample area of 10 mm × 10 mm. For t_A, a setup time of 30 min before LPM and 10 min before measuring the samples is calculated for each batch of process parameter sets with the number of parameter sets K. In addition, a measurement time of 45 s per process parameter set k for WLI is recorded. t_C is then accumulated across all batches. The calculation of t_C, t_P, and t_A is performed as follows:

$$t_C = \sum_{k=1}^{K} \frac{t_{P,k}}{3600} + t_A;\ t_P = \frac{10\ mm}{v_s} \cdot \frac{10\ mm}{0{,}001 \cdot dy} \cdot n;\ t_A = 0{,}5 + 0{,}1667 + 0{,}0125 \cdot K;\ [t_c, t_N] = h, [t_P] = s \qquad (4)$$

Using the benchmark framework outlined above, the sequential variation LPM-PPD strategy based on domain knowledge is compared against the state of art DOE strategy. The latter refers to design space optimization using all process parameter dimensions simultaneously as is the most common strategy described in literature for LPM. The digitized LPM-PPD strategies are implemented using Python version 3.13.

Two boundary conditions are set for benchmarking: a target roughness and a maximum number of experiments. To achieve a reduction in initial roughness suitable for most industry inquiries, Sa-S = 0.2 µm is defined as the target roughness. The maximum number of experiments is set at 50. This limits the effort required for the corresponding real experimental investigations to one person-day. Additionally, this aligns with the number of experiments that is most often used in literature employing DOE.

First, the strategies are compared solely based on the minimal Sa-S values in relation to t_C of the LPM-PPD. Then multi-objective optimization is analyzed. To select the most suitable process parameter set, a weighted sum of the values of Sa-S, Sa-L and t_P is calculated. The weights are recorded in the target vector and varied in the following steps: [(0.7, 0.15, 0.15); (0.5,0.25,0.25); (0.5,0.1,0.4)], where (0.7, 0.15, 0.15) refers to 70% weight to Sa-S, 15% weight to Sa-L and 15% weight to t_P.

An algorithm is developed to digitize the LPM-PPD strategy based on domain knowledge for sequential variation. This algorithm includes the sequence of variation, the process parameter space, and the adjustment of the process parameter dimensions during successive iterations as described in section 2.4. The variation of individual process parameter dimensions

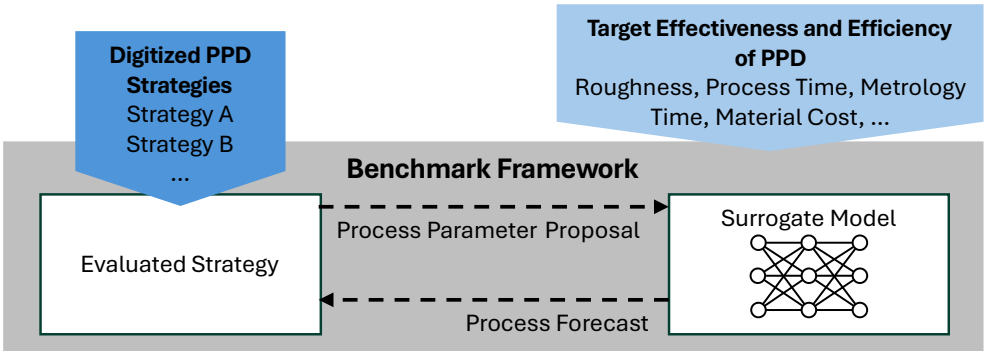

Figure 6: Schematic representation of the benchmark framework with external boundary conditions and selection of the PPD strategy.

is executed within a loop until the respective target value is met. If this target cannot be met, the algorithm returns to a previously examined process parameter dimension. For example, d_L is increased after an ineffective investigation of P_L and v_s in a new iteration.

For evaluation of the LPM-PPD strategy based on domain knowledge, a variation of the starting process parameter set is examined in separate runs of the sequential variation: d_L = [100, 150, 250, 400, 600] µm with $dy = 0.25 \times d_L$, and n = 2. P_L and v_s for the "rough" variation are then selected by the algorithm. In the "rough" variation a reduction in initial roughness of 75% (initial value: Sa-S = 1,57 µm) is targeted. In the ensuing "fine" variation of P_L and v_s the target of Sa-S = 0.2 µm is tracked.

Additionally, two runs of the LPM-PPD strategy based on DOE are evaluated. In the first run, the process parameter space investigated by DOE is restricted through use of domain knowledge. For the second run, the domain knowledge is withheld. Both runs of the LPM-PPD strategy based on DOE are composed of two respective batches of process parameter sets. For the first batch, a face-centered central composite design with 15 parameter combinations is applied. Different levels for variation of d_L, P_L, and v_s are chosen with constant dy and n. In each instance of the second batch of process parameter sets, the respective determined local optimum is used to create a full-factorial DOE with 35 entries. d_L is no longer varied to keep a constant melt pool width, whilst P_L, v_s, dy, and n are varied to balance melt pool width, repeated local remelting and processing time simultaneously. Table 6 gives an overview of the two individual runs of two-stage DOE.

Table 6. Overview of the variation of process parameters and levels for the two benchmarked runs of LPM-PPD based on DOE.

DOE with domain knowledge						
	d_L in µm	**P_L in W**	**v_s in mm/s**	**dy in µm**	**n**	**DOE type**
1. batch	[150, 250, 400]	[50, 125, 200]	[25, 100, 175]	0.25× d_L	2	Central composite
2. batch	$d_{L,batch1}$	[0.8333 × $P_{L,batch1}$, $P_{L,batch1}$, 1.2 × $P_{L,batch1}$]	[$v_{s,batch1}$, 1.5 × $v_{s,batch1}$]	[0.25, 0.2, 0.1] × $d_{L,batch1}$	[2, 4]	Full factorial
DOE without domain knowledge						
	d_L in µm	**P_L in W**	**v_s in mm/s**	**dy in µm**	**n**	**DOE type**
1. batch	[100, 400, 600]	[50, 275, 500]	[25, 162.5, 300]	0.25× d_L	2	Central composite
2. batch	$d_{L,batch1}$	[0.8333 × $P_{L,batch1}$, $P_{L,batch1}$, 1.2 × $P_{L,batch1}$]	[$v_{s,batch1}$, 1.5 × $v_{s,batch1}$]	[0.25, 0.2, 0.1] × $d_{L,batch1}$	[2, 4]	Full factorial

4. Results and discussion

Figure 7 shows the progression of the Sa-S value against the accumulated cycle time during the LPM-PPD: (a) shows the results of the algorithm for sequential variation, (b) shows the results of the strategy based on DOE. The target value of the LPM-PPD of Sa-S ≤ 0.2 µm is indicated by a red, horizontal line. Only a section up to Sa-S ≤ 0.4 µm is shown to better distinguish the individual markings. Respectively, the initial roughness of Sa-S = 1.57 µm is cut off. Each starting process parameter set is assigned to a specific color in (a). The respective current locally optimal process parameter set of the LPM-PPD is marked as a data point in color of the starting point. The laser beam diameter, which is subject to change during a run, is assigned an individual symbol. An overview of the symbols for d_L is shown in the legend.

Above all, it is shown that the developed benchmarking framework is effective. The surrogate model can be used with different digitized strategies to adapt and determine process parameter sets in various iterations for a specified target. Figure 7 (a) shows that the developed algorithm for sequential variation adapts the process parameters dimensions effectively. The target of Sa-S = 0.2 µm is achieved for all tested initial values except d_L = 100 µm. The algorithm for sequential variation shows a trend to converge to d_L = 250 µm and each adjustment of d_L in this direction between batches further reduces Sa-S. Thus, the algorithm for sequential variation compensates for suboptimal starting process parameter sets and shows high robustness against a suboptimal starting process parameter set. The lowest roughness, Sa-S = 0.1050 µm, is reached after calculated cycle time t_C = 5.8968 h. In Table 7 the determined process parameter sets per strategy are listed.

Figure 7 (b) shows that Sa-S = 0.2 µm is met in both DOE variants – one using domain knowledge and one without. Using domain knowledge, the DOE reaches a much lower roughness then the DOE without domain knowledge and d_L = 250 µm is selected. A process parameter set for Sa-S = 0.105 µm is identified after just t_C = 2.88 h. Whilst overall a smaller t_C is calculated than using the developed algorithm for sequential variation, the time between batches is increased and therefore

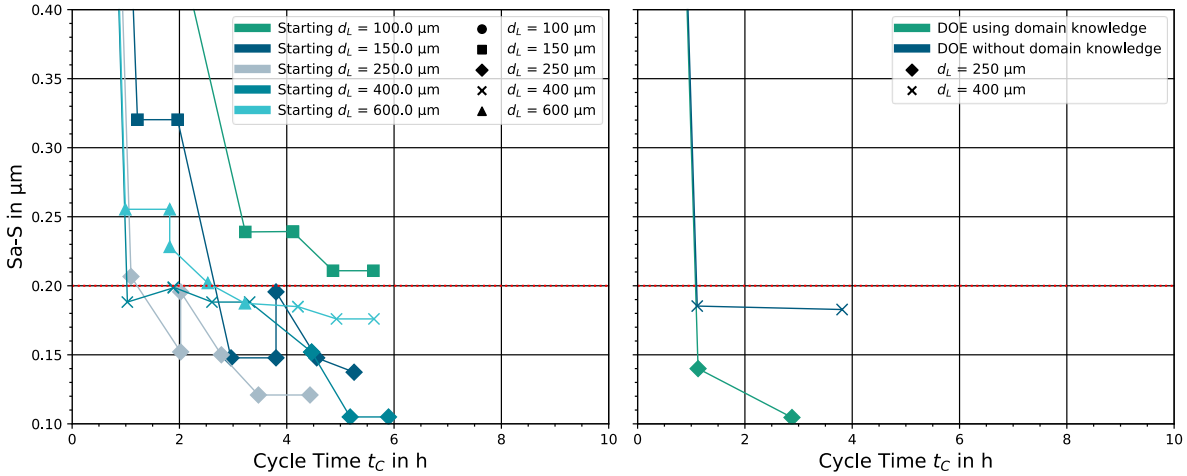

Figure 7: Sa-S value against the accumulated cycle time of LMP-PPD targeting Sa-S = 0.2 µm for different starting process parameter sets. (a) Algorithm for sequential variation and (b) two runs of DOE. Max. 50 investigated process parameter sets.

the efficiency per batch is decreased. Without domain knowledge, the DOE yields only one parameter set with Sa-S = 0.182 µm. In this case, d_L = 400 µm is used, and the second DOE batch does not further reduce roughness.

Table 7. Process parameter sets determined by LPM-PPD strategies benchmarked in this study targeting reduction in initial roughness.

LPM-PPD strategy	d_L **in µm**	P_L **in W**	v_s **in mm/s**	dy **in µm**	n	t_P **in s**	**Sa-S in µm**
Algorithm for sequential variation	250	156	125	25	2	64	0.105
DOE with domain knowledge	250	104	100	62.5	4	64	0.105
DOE without domain knowledge	400	275	37.5	100	2	53	0.182

Figure 8 shows the results utilizing a target vector with weights for Sa-S, Sa-L, and t_P, simulating multi-objective optimization. In Figure 8 (a) and (b), the Sa-S value predicted after the LPM-PPD, and in (c) and (d) the calculated $t_P$for the respective process parameter sets are plotted against the variation of the target vector. Figure 8 (a) and (c) show the results for the use of the developed algorithm for sequential variation and (b) and (d) for the use of DOE.

Figure 8 (a) and (b) demonstrate that decreasing weight assigned to Sa-S in the target vector results in a higher predicted value of Sa-S after LPM-PPD. The lowest values of Sa-S over all are predicted when specifying a target vector of (1, 0, 0). It is shown that a weight greater than 0.7 must be assigned to Sa-S to reach the target 0.2 µm in all tested instances. Lastly, with a weight of 0.5 for Sa-S the target roughness is only achieved using DOE on a parameter space restricted by domain knowledge (Figure 8 (b)) where a weight of 0.4 can be assigned to t_P. Figure 8 (c) and (d) show that using a target vector in the benchmark framework is an effective method for implementing multi-objective optimization without an increase in computing time. With an increasing weight assigned to Sa-S, t_P of the determined process parameter sets is reduced, both when using the algorithm for sequential variation as well as in the DOE runs. The trend toward a decrease in t_P results in a corresponding trend toward an increase in Sa-S. The lowest values of t_P are calculated for weights of (0.5, 0.1, 0.4).

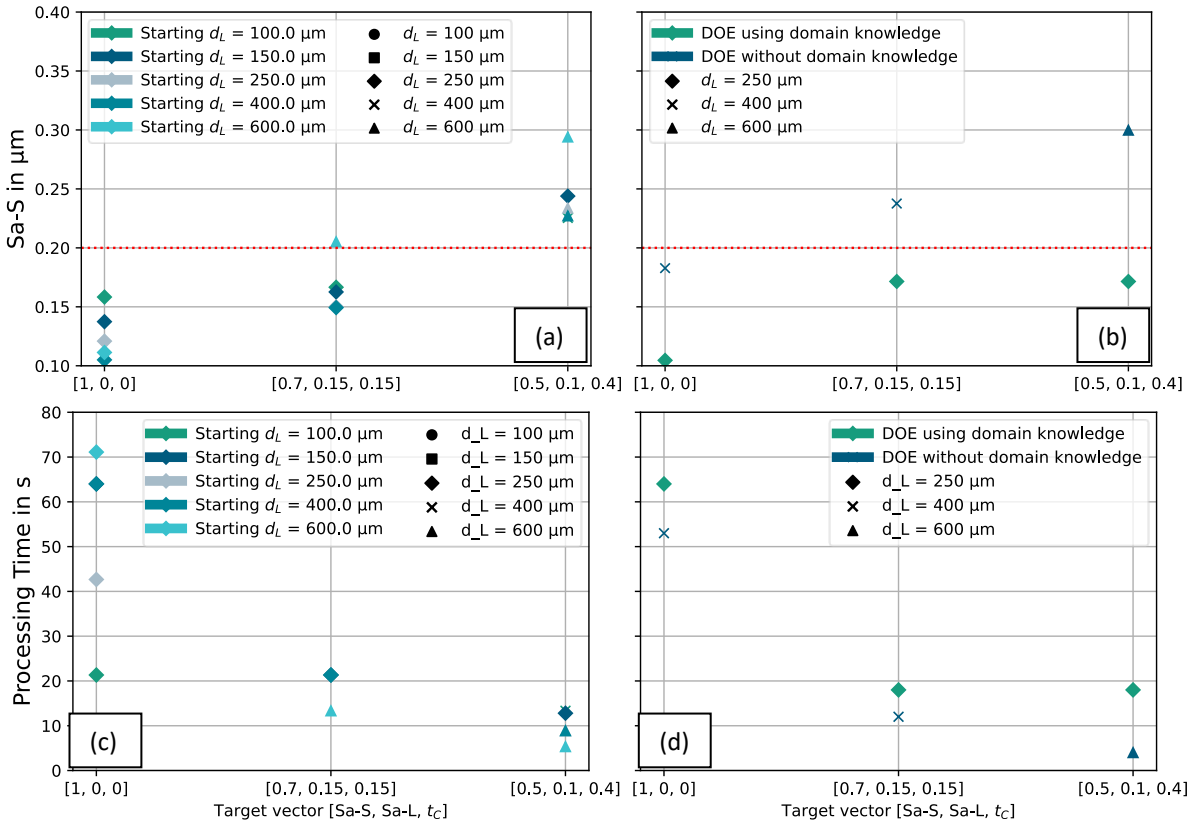

Figure 8: (a) and (b) Sa-S value predicted after LPM-PPD against variation of target vector determining weights for [Sa-S, Sa-L, t_P]. (c) and (d) corresponding t_C against variation of target vector. Max. 50 investigated process parameter sets.

5. Summary and outlook

In this work a surrogate model for laser polishing of AISI H11 is developed to replace real-world experimental investigations. In combination with digitized process parameter development strategies for laser polishing of metals, a framework for benchmarking these strategies based on the low-cost surrogate model is created and validated. In the benchmark framework, the evaluated LPM-PPD strategy suggests process parameter sets to the surrogate model which returns a prediction of the resulting surface roughness. Boundary conditions can be specified to restrict the strategy, for example target roughness or the maximum number of investigated process parameter sets. The effectiveness, measured by achieved roughness, and the efficiency, based on the accumulated cycle time of LPM-PPD, are determined for each strategy by the benchmark framework. Since each run of a strategy using the surrogate model is significantly faster than real-world experiments and almost cost-free, entire virtual LPM-PPD campaigns can be completed in seconds instead of weeks. This for the first time enables systematically comparing alternative LPM-PPD strategies in different scenarios (e.g., limited number of test material, limited cycle time, minimal target roughness).

The surrogate model is based on a multi-layer perceptron which is trained on 2560 measured process parameter sets. It predicts the surface roughness value Sa with an RMSE of 0.16 µm and median relative model error of 9.32 % across the entire roughness range of the data set.

Using the benchmark framework, two LPM-PPD strategies are compared. For the first strategy, an algorithm is developed digitizing LMP-PPD based on extensive domain knowledge distilled from two dissertations. As domain knowledge, the methodology of process experts on LPM is listed explicitly, including sequencing, limits and adjustment of process parameter dimensions. In this domain knowledge, the individual influence of the process parameter dimensions beam diameter d_L, laser power P_L and scanning speed v_S, track offset dy, and number of passes n on LPM is recorded. The second strategy is based on two types of a two-stage design of experiments (DOE), resembling the reported state of the art for LPM-PPD. For the first type of DOE, the searched process parameter dimensions are restricted based on the recorded domain-knowledge

of given material. The second type of DOE searches the full parameter space recorded within the data set on which the surrogate model is developed.

The LPM-PPD strategy based on domain knowledge consistently reaches the target roughness (Sa-S ≤ 0.2 µm) in fewer than 50 “virtual” experiments, even when it starts from deliberately far from optimal parameter sets (variation of laser beam diameter as starting process parameter). The process parameter dimensions are adjusted effectively between batches of process parameter sets and d_L converges to an optimum in accordance with the state of the art. A minimal roughness of Sa-S = 0.105 µm is predicted for the most optimal of determined process parameter set. The same roughness can be achieved by LPM-PPD based on DOE – but only if the process parameter dimensions are restricted to favourable areas based on domain knowledge. Therefore, it is shown that domain knowledge in sequential variation as well as DOE for process parameter dimensions is pivotal for balancing effectiveness and efficiency in LPM-PPD.

Through the evaluation of these LPM-PPD strategies it is shown that differing respective efficiency and effectiveness can be determined. Multiple runs of different LPM-PPD strategies are completed effectively through the interaction of the digitized strategies and the surrogate model. Thereby, the developed benchmark framework is validated. Additionally, it is shown that a multi-objective optimization of process parameter sets can be realised using the weighted sum to compute an auxiliary target value from several objectives (e.g., surface roughness, surface waviness, areal processing time). Respective process parameter sets are determined flexibly without retraining the surrogate model or increasing computation time.

In future work, the established methodology should be expanded to include further materials, initial surface profiles and machine configurations. Additionally, the benchmark framework should be adapted to determine subsequent process parameter sets for a second step of macro-polishing or a step of micro-polishing in accordance with the state of the art.

Furthermore, the developed benchmark framework should be used to evaluate additional LPM-PPD strategies based on machine learning methods, such as Bayesian Optimization or evolutionary algorithms such as particle swarm optimization. Consequently, the findings should be used to drive automation of LPM-PPD. A real-time recommendation of process parameters, considering machine-specific limits and cost models, further industrializes the usage of laser polishing of metals. Regarding the surrogate modelling, an interesting direction for future work is to investigate whether the surrogate model can be effectively trained on significantly less data with minimal loss in accuracy. Additionally, it would be valuable to explore whether the learned feature space can be efficiently adapted to new materials or different surface roughness conditions with a reduced number of experiments.

References

ZENG, X., G. ZHU, Z. GAO, R. JI, J. ANSARI und C. LU. *Surface polishing by industrial robots: a review [online]*. In: *The International Journal of Advanced Manufacturing Technology,* 2023, 125(9-10), p. 3981-4012. ISSN 1433-3015.

GISARIO, A., M. BARLETTA und F. VENIALI. *Laser polishing: a review of a constantly growing technology in the surface finishing of components made by additive manufacturing [online]*. In: *The International Journal of Advanced Manufacturing Technology,* 2022, 120(3), p. 1433-1472. ISSN 1433-3015.

WILLENBORG, E.: *Polieren von Werkzeugstählen mit Laserstrahlung,* Aachen, Techn. Hochsch., Diss., 2005. Aachen, Shaker, 2006. Berichte aus der Lasertechnik. ISBN 383224896X.

TEMMLER, A., D. LIU, J. PREUßNER, S. OESER, J. LUO, R. POPRAWE und J.H. SCHLEIFENBAUM. *Influence of laser polishing on surface roughness and microstructural properties of the remelted surface boundary layer of tool steel H11 [online]*. In: *Materials & Design,* 2020, 192, p. 108689. ISSN 02641275.

KIEDROWSKI, T.: *Oberflächenstrukturbildung beim Laserstrahlpolieren von Stahlwerkstoffen,* Aachen, Techn. Hochsch., Diss., 2009. Aachen, Shaker, 2009. Berichte aus der Lasertechnik. ISBN 9783832287412.

KUMSTEL, J.: *Steigerung der Flächenrate beim Laserpolieren von Stahlwerkstoffen,* Aachen, Tech. Hochsch., Diss., 2021.

WANG, G. Gary; Shan, S. (2007): Review of Metamodeling Techniques in Support of Engineering Design Optimization. In: *J. Mech. Des* 129 (4), p. 370–380.

SIMPSON, T. W.; Poplinski, J. D.; Koch, P. N.; Allen, J. K. (2001): Metamodels for Computer-based Engineering Design: Survey and recommendations. In: *EWC* 17 (2), p. 129–150.

FORRESTER, Alexander I. J.; Sóbester, András; Keane, Andy J. (2008): Engineering design via surrogate modelling. A practical guide. Chichester, Hoboken, N.J: John Wiley distributor; Wiley.

BHOSEKAR, A., & IERAPETRITOU, M. (2018). Advances in surrogate based modeling, feasibility analysis, and optimization: A review. *Computers & Chemical Engineering*, **108**, p. 250–267.

MIŠIĆ, V. (2020). Optimization of tree ensembles. *Operations Research*, **68**(5), 1423–1438.

FISCHETTI, M., & JO, J. (2018). Deep neural networks and mixed integer linear optimization. *Constraints*, **23**(3), p. 296–309.

GRIMSTAD, I., & ANDERSSON, H. (2019). ReLU networks as surrogate models in mixed-integer nonlinear programming. *Computers & Chemical Engineering*, **131**, 106580.

BERTSIMAS, D., Gupta, V., & Kallus, N. (2010). Robust sample average approximation. *Mathematical Programming*, **171**, p. 217–282.

WILSON, A. G., Hu, Z., Salakhutdinov, R., & Xing, E. P. (2020). Deep kernel learning. *Artificial Intelligence and Statistics*, 370–378. Bhosekar, A., & Ierapetritou, M. (2018). Advances in surrogate based modeling, feasibility analysis, and optimization: A review. *Computers & Chemical Engineering*, **108**, p. 250–267.

MCBRIDE, Kevin; SUNDMACHER, Kai (2019): Overview of Surrogate Modeling in Chemical Process Engineering. In: *Chemie Ingenieur Technik* 91 (3), p. 228–239.

MISENER, Ruth; BIEGLER, Lorenz (2023): Formulating data-driven surrogate models for process optimization. In: *Computers & Chemical Engineering* 179, p. 108411.

DIN EN ISO 25178-1:2016-12, Geometrische Produktspezifikation (GPS) - Oberflächenbeschaffenheit: Flächenhaft - Teil 1: Angabe von Oberflächenbeschaffenheit (ISO 25178-1:2016); Deutsche Fassung EN ISO 25178-1:2016

DIN EN ISO 21920-3:2022-12, Geometrische Produktspezifikation_(GPS)_- Oberflächenbeschaffenheit: Profile_- Teil_3: Spezifikationsoperatoren (ISO_21920-3:2021); Deutsche Fassung EN_ISO_21920-3:2022. Berlin, DIN Media GmbH.

UKAR, E., A. LAMIKIZ, L.N. LO´PEZ DE LACALLE, F. LIEBANA und J.M. ETAYO. *Laser Polishing Parameter Optimization for Die and Moulds Surface Finishing [online]*. In: *Proceedings of the ASME International Manufacturing Science and Engineering Conference, 2008,* 2008, p. 197-204

KUMAR, A., H. RAMADAS, C.S. KUMAR und A.K. NATH. *Laser polishing of additive manufactured stainless-steel parts by line focused beam: A response surface method for improving surface finish [online]*. In: *Journal of Manufacturing Processes,* 2025, 133, p. 1310-1328. ISSN 15266125.

SOLHEID, J.S., A. ELKASEER, T. WUNSCH, A.P. CHARLES, H.J. SEIFERT und W. PFLEGING. *Effect of process parameters on surface texture generated by laser polishing of additively manufactured Ti-6Al-4V [online]*. In: *Proc. SPIE 11268, Laser-based Micro- and Nanoprocessing XIV,* 2020, (11268), p. 112680Q.

ROSA, B., J.Y. HASCOET und P. MOGNOL. Modeling and Optimization of Laser Polishing Process [online]. In: Applied Mechanics and Materials, 2014, 575, p. 766-770. ISSN 1662-7482.

MEYLAN, B., I. CALDERON und K. WASMER. Optimization of Process Parameters for the Laser Polishing of Hardened Tool Steel [online]. In: Materials, 2022, 15(21). ISSN 1996-1944.

UKAR, E., A. LAMIKIZ, S. MARTÍNEZ, I. TABERNERO und L.L. de LACALLE. *Roughness prediction on laser polished surfaces [online]*. In: *Journal of Materials Processing Technology,* 2012, 212(6), S. 1305-1313. ISSN 09240136.

SOLHEID, J.S., A. ELKASEER, T. WUNSCH, S. SCHOLZ, H.J. SEIFERT und W. PFLEGING. *Multiobjective Optimization of Laser Polishing of Additively Manufactured Ti-6Al-4V Parts for Minimum Surface Roughness and Heat-Affected Zone [online]*. In: *Materials,* 2022, 15(9). ISSN 1996-1944.

MEYLAN, B., A. MASSEREY, E. BOILLAT, I. CALDERON und K. WASMER. *Thermal Modelling and Experimental Validation in the Perspective of Tool Steel Laser Polishing [online]*. In: *Applied Sciences,* 2022, 12(17). ISSN 2076-3417.

PHAM, D.-P. und H.-C. TRAN. *Multi-physics simulation for predicting surface roughness of laser powder bed fused parts after laser polishing [online]*. In: *Additive Manufacturing,* 2024, 94, p. 104486. ISSN 22148604.